JOURNAL OF MATERIALS SCIENCE 30 (1995) 1158–1165

Some properties of mullite powders prepared by chemical vapour deposition

Part I *Preparation of mullite powder*

K. ITATANI, T. KUBOZONO, F. S. HOWELL, A. KISHIOKA, M. KINOSHITA
Department of Chemistry, Faculty of Science and Engineering, Sophia University, 7-1 Kioi-cho, Chiyoda-ku, Tokyo 102, Japan

The chemical vapour deposition (CVD) technique based upon reaction among aluminium chloride ($AlCl_3$), silicon chloride ($SiCl_4$) and oxygen was applied to produce submicrometre-sized mullite ($3Al_2O_3 \cdot 2SiO_2$) powder. The conditions for preparing the best crystalline mullite were as follows: (i) the reaction temperature, 1200 °C; (ii) the flow rate of carrier gas (Ar) of $AlCl_3$, 0.3 $dm^3 min^{-1}$, and that of $SiCl_4$, 0.3 $dm^3 min^{-1}$; (iii) the sublimation temperature of $AlCl_3$, 180 °C, and the evaporation temperature of $SiCl_4$, 25 °C; and (iv) the flow rate of oxygen, 0.9 $dm^3 min^{-1}$. The as-prepared powder contained mullite, a small amount of γ-Al_2O_3 (Al–Si spinel) and amorphous material; this powder was composed of spherical primary particles of $\sim$ 0.05 μm diameter. Although only mullite was present at the calcination temperature of 1300 °C, a small amount of α-Al_2O_3 was formed at 1400–1700 °C. Agglomeration due to primary particle growth started at temperatures exceeding 1400 °C.

1. Introduction

High purity and dense mullite ($3Al_2O_3 \cdot 2SiO_2$) ceramics exhibit significant properties, such as high thermal resistance (incongruent melting at 1828 $\pm$ 10 °C) [1], low thermal expansion coefficient ($\alpha(a) = 3.9 \times 10^{-6}\,°C^{-1}$; 300–900 °C) [2] and great bending strength (360–370 MPa; RT $\sim$ 1300 °C) [3]. Various techniques have been developed to produce high purity and easily sinterable mullite powder: alkoxide [4], spray pyrolysis [3, 5], coprecipitation [6] and chemical vapour deposition (CVD) [7–9].

Among these techniques, CVD has many advantages for preparing mullite powder with little agglomeration, submicrometre-sized primary particles, and regular particle shapes. Although plasma CVD [7] and flame CVD [8, 9] have been utilized to prepare mullite powder, crystalline mullite could not be obtained until the as-prepared powder, containing amorphous material, was heated up to $\sim$ 1000 °C. Thus little information on the direct precipitation of crystalline mullite by CVD has been available until now, and the properties of the resulting powder are not reported. This paper describes: (i) the preparation conditions for the crystalline mullite powder by CVD, and (ii) some properties of the as-prepared and calcined powders.

2. Experimental procedure

2.1. Reaction apparatus and preparation of powder

An overall view of the reaction apparatus is shown in Fig. 1. The reaction apparatus is composed of:

(i) a vaporization zone of aluminium chloride ($AlCl_3$) and silicon chloride ($SiCl_4$);

(ii) a reaction zone among $AlCl_3$, $SiCl_4$ and oxygen (O_2); and

(iii) a collection zone of the resulting powder.

Each zone is explained below.

2.1.1. Vaporization of $AlCl_3$ and $SiCl_4$

The $AlCl_3$ powder (a), Fig. 1, was sublimed at 180 °C using a mantle heater (b); whereas the $SiCl_4$ solution (c) was evaporated at 25 °C in an oil bath (d); these vaporization temperatures were chosen to form stoichiometric mullite, taking evaporation pressures into consideration.

2.1.2. Formation of powder

The $AlCl_3$ vapour, $SiCl_4$ vapour and oxygen (e), Fig. 1, were introduced into a fused silica tube with i.d. 60 mm and length 1 m (g); $AlCl_3$ and $SiCl_4$ vapours were transferred to the tube, using argon (Ar) gas as a carrier gas. The flow rate ratios of the carrier gas for $AlCl_3$ [Ar($AlCl_3$)] and for $SiCl_4$ [Ar($SiCl_4$)] were 0.3:0.3, 0.6:0.6 and 0.9:0.9 $dm^3 min^{-1}$:$dm^3 min^{-1}$ respectively; the flow rate of oxygen (O_2) gas was fixed at 0.9 $dm^3 min^{-1}$. The reaction temperatures in the electric furnace (h) were monitored using Pt–Pt13Rh thermocouples (f), Fig. 1.

2.1.3. Collection of powder

The powder was collected using a test-tube type filter (i); the evolved gas was trapped in an Erlenmeyer flask

0022–2461

with concentrated sodium hydroxide [NaOH; (j)], using an aspirator (k), Fig. 1. The yield of the resulting powder was ~ 78% of the theoretical value.

2.2. Phase identification and quantitative analysis

The phase identification of the resulting powder was conducted using an X-ray diffractometer with Cu$K\alpha_1$ radiation operated at 40 kV and 25 mA (model Rad II A, Rigaku, Tokyo) and using an infrared (i.r.) spectrometer (model 260–50, Hitachi, Tokyo) with KBr-pellet technique. The cell dimensions of mullite were determined using (2 2 0), (1 1 1) and (1 2 1) reflections. Differential thermal analysis (DTA) of the powder, with a sample weight of 50 mg, was carried out in air at a heating rate of 10 °C min^{-1}. The Al_2O_3, SiO_2 and Cl contents were determined quantitatively using an X-ray fluorescence apparatus (model SXF-1200, Shimadzu, Kyoto).

2.3. Examination of powder properties

The specific surface area of the resulting powder was measured by the Brunauer–Emmett–Teller (BET) technique, using nitrogen (N_2) as the adsorption gas; the true density of the powder was measured picnometrically.

The crystallite size, G_{XRD} [(1 2 1) reflection], was examined according to Scherrer's formula. The primary particle size, G_{BET}, was calculated by assuming the particles to be spherical; the secondary particle size, G_{LSA}, was obtained using a laser scattering analyser (model LA-700, Horiba, Kyoto).

The particle shape was observed using a transmission electron microscope (TEM; models H-300 and H-9000NA, Hitachi, Tokyo) and a scanning electron microscope (SEM; model S-430, Hitachi, Tokyo).

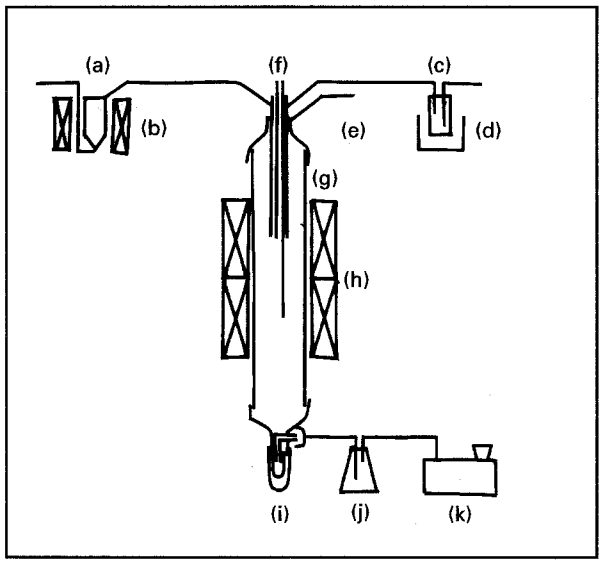

Figure 1 Schematic diagram of the reaction apparatus: (a) $AlCl_3$ powder, (b) mantle heater, (c) $SiCl_4$ solution, (d) oil bath, (e) oxygen, (f) thermocouple, (g) fused silica tube (i.d. 60 mm; length, 1 m), (h) electric furnaces, (i) test-tube type filter, (j) Erlenmeyer flask filled with saturated sodium hydroxide (NaOH), (k) aspirator.

The agglomeration strength was examined by measuring the dimensions of the compact fabricated by pressing the powder, of 0.30 g weight, in steel dies (i.d. 10 mm).

3. Results and discussion

3.1. Properties of the as-prepared powders

The optimum conditions for preparing the crystalline mullite are explained, and the properties of the as-prepared powders are reported in this section.

3.1.1. Crystalline phases

Fig. 2 shows the X-ray diffraction patterns of the as-prepared powders. First, the effect of reaction temperature on phase formation was examined by fixing the Ar($AlCl_3$)/Ar($SiCl_4$) ratio to a minimum, i.e. 0.3:0.3. Not only poorly crystalline $AlCl_3 \cdot 6H_2O$ [10], but also amorphous material was present at 900 °C. Mullite [11] was detected at 1000, 1100 and 1200 °C, together with a small amount of γ-Al_2O_3 [12]; the higher the reaction temperature was, the better the crystallinity of mullite became. Second, the effect of flow rate of the Ar gas, Ar($AlCl_3$)/Ar($SiCl_4$), was examined by fixing the reaction temperature at a maximum, i.e. 1200 °C. The higher the flow rate of the Ar gas, the poorer the crystallinity of mullite became; amorphous material, as well as $AlCl_3 \cdot 6H_2O$, was present at Ar($AlCl_3$)/Ar($SiCl_4$) = 0.9:0.9.

It is noteworthy that crystalline mullite may be formed directly by the CVD present, because the amorphous material is the only, or the major, phase present in the cases of plasma CVD [7] and flame CVD [8, 9]. The optimum conditions for preparing the crystalline mullite are as follows: reaction temperature, 1200 °C; flow rate of Ar($AlCl_3$), 0.3 dm^3 min^{-1}, and that of Ar($SiCl_4$), 0.3 dm^3 min^{-1}. These conditions indicate that higher reaction temperature and longer residence time of the vaporized materials in the electric furnaces may promote crystal growth of mullite. The residence time in the electric furnaces is, for example, estimated to be ~ 30 s when the Ar flow rate is 0.9 dm^3 min^{-1}; whereas it extends to ~ 90 s when

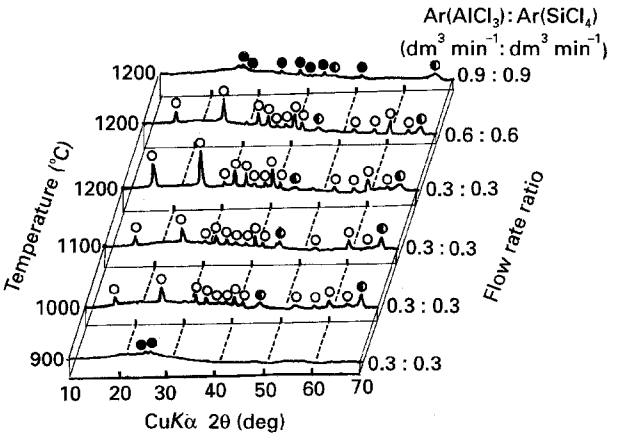

Figure 2 X-ray diffraction patterns of the as-prepared powders as functions of reaction temperature and flow-rate ratios of carrier gas (Ar) for $AlCl_3$ and $SiCl_4$: (○) mullite, (◐) γ-Al_2O_3, (●) $AlCl_3 \cdot 6H_2O$.

the Ar flow rate is 0.3 $dm^3 min^{-1}$. The formation of $AlCl_3 \cdot 6H_2O$ at the lowest reaction temperature, i.e. 900 °C, and at the highest Ar flow rate, i.e. 0.9:0.9, seems to be due to hydration of undecomposed $AlCl_3$. On the basis of the XRD results, the properties of the powder of the best crystalline mullite, prepared under optimum conditions, are described below.

The composition of the as-prepared powder was first determined using X-ray fluorescence apparatus. The Al_2O_3 and SiO_2 contents were 72.70 and 27.23%, respectively; the Cl content was 0.07%.

The Al_2O_3 and SiO_2 contents are close to those of stoichiometric mullite (Al_2O_3, 71.79%; SiO_2, 28.21%) and are in the range of the mullite composition [1, 13]. As the detection of γ-Al_2O_3 by XRD indicates, amorphous SiO_2 must be present to keep the mullite composition; most of this SiO_2 may exist in solid solution in γ-Al_2O_3 to form Al–Si spinel, whose composition is estimated to be $(\square_{4-x}Al_{16-x})^{iv}(\square_xAl_xSi_4)^{iv}O_{32}$, where $\square$ equals vacancy [14], $6Al_2O_3 \cdot SiO_2$ [15] or $3Al_2O_3 \cdot 2SiO_2$ [16]. The Cl content of the reaction product is as low as 0.07%, regardless of the use of $AlCl_3$ and $SiCl_4$ as starting sources. This value is lower than the value (2%) of flame CVD [9]; such a low value may be attributed to the residence time ($\sim$ 90 s) of the vaporized materials in the electric furnaces being longer than in the case of flame CVD.

3.1.2. The powder's properties

Specific surface area, primary particle size, crystallite size and true density were measured to establish the CVD powder's properties. The properties of the as-prepared powder were as follows: specific surface area, 43.5 $m^2 g^{-1}$; primary particle size, 0.046 μm; crystallite size, 0.045 μm; true density, 3.00 $g cm^{-3}$.

The properties of the powder prepared by flame CVD are reported as follows: specific surface area, 54.6 $m^2 g^{-1}$; primary particle size, 0.038 μm; true density, 2.863 $g cm^{-3}$ [17]. The present as-prepared powder has thus lower surface area, larger primary particle size, and higher true density than the powder prepared by flame CVD. The difference in powder properties between this CVD and flame CVD may result from the residence time in the hot zone, because the residence time ($\sim$ 90 s) of the present CVD is much longer than that ($\sim$ 65 ms) of flame CVD [8].

Fig. 3 shows the TEM image and the particle size distribution of the as-prepared powder. The particle shape was spherical, Fig 3a, and the spheres had diameters in the range 0.01–0.12 μm (the average diameter was 0.05 μm, Fig. 3b).

The spherical particles correspond to primary particles, because the particle sizes observed by TEM are in accord with the primary particle size (0.046 μm). These primary particles disperse with little agglomeration, which is a feature of the powder prepared by CVD.

3.2. Properties of the calcined powders

As shown in Section 3.1., the best crystalline mullite was obtained under the following conditions: (i) with a reaction temperature of 1200 °C, and (ii) with a carrier gas (Ar) flow rate for $AlCl_3$ of 0.3 $dm^3 min^{-1}$, and that for $SiCl_4$ of 0.3 $dm^3 min^{-1}$: changes in the powders' properties with calcination temperature are described below.

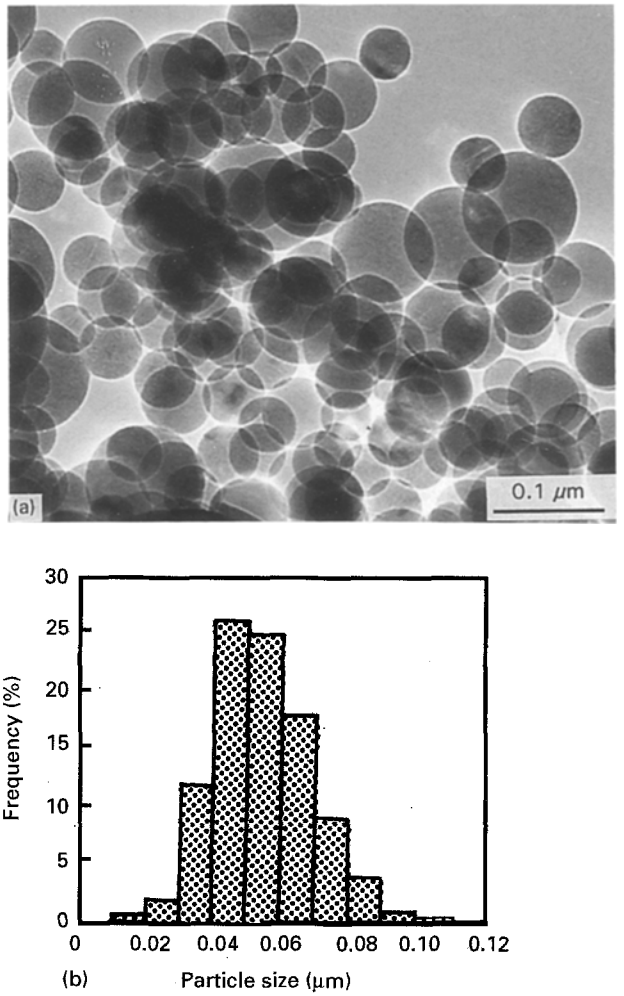

Figure 3 (a) TEM micrograph and (b) particle size distribution of the as-prepared powder: Reaction temperature, 1200 °C; flow rate ratio, $Ar(AlCl_3)/Ar(SiCl_4) = 0.3\ dm^3 min^{-1} : 0.3\ dm^3 min^{-1}$.

3.2.1. Phase changes during calcination

First, DTA of the as-prepared powder was performed from room temperature to 1400 °C. Although the data were omitted in this paper, a very weak exothermic effect appeared at 920–950 °C.

The phase changes during calcination were then examined by XRD and i.r. Fig. 4 shows the XRD patterns of the calcined powders. Not only mullite, but also a small amount of γ-Al_2O_3 (Al–Si spinel) was present at temperatures between 900 and 1200 °C; however, neither θ- nor δ-Al_2O_3 was found in the calcined powders. Although only mullite was detected at 1300 °C, a small amount of α-Al_2O_3 [18], together with mullite, was present above 1400 °C. Splitting of the (2 1 0) and (1 2 0) reflections, $2\theta = 26.3$ and 26.0° respectively, in the mullite phase took place at and above 1300 °C.

Fig. 5 shows the i.r. spectra of the as-prepared and calcined powders. The absorption peaks of the as-prepared powder Fig. 5a, appeared at 1120, 820, 730

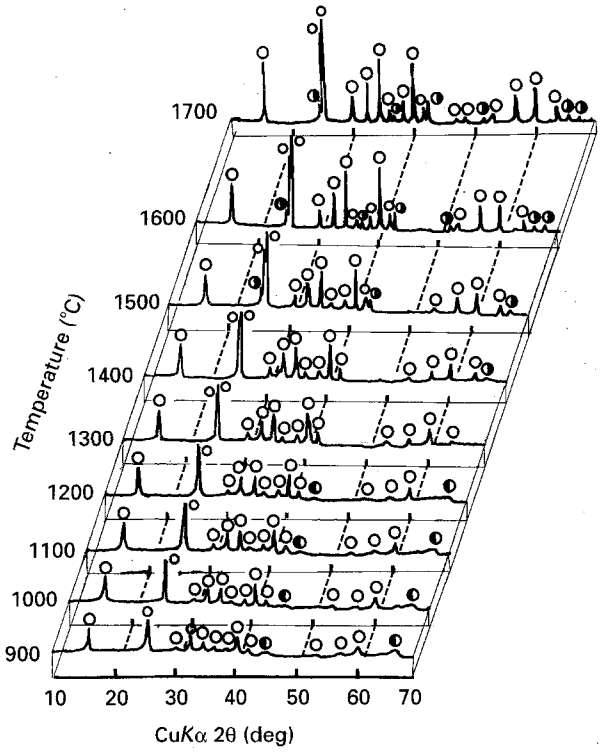

Figure 4 XRD patterns of the powders calcined at various temperatures for 1 h: heating rate, 10 °C min^{-1}; (○) mullite; (◐) γ-Al_2O_3; (◑) α-Al_2O_3.

and 590 cm^{-1}. The absorption peak at 1120 cm^{-1} may be assigned to the SiO_4 unit (Si–O), the peaks at 820 and 590 cm^{-1} to the AlO_6 unit (O–Al–O), and the peak at 730 cm^{-1} to the AlO_4 unit (O–Al–O) [19]. An additional absorption peak at 1170 cm^{-1} appeared in the powder calcined at 1200 °C (see arrow mark, Fig. 5b); the absorption peak at 1120 cm^{-1} became weaker than that of 1170 cm^{-1} at 1300 °C, Fig. 5c–f. The absorption peak at 1170 cm^{-1} may be assigned to the AlO_4 unit (Al–O) [19]. At and above 1400 °C, the 460 cm^{-1} peak appeared in the i.r. spectra, Fig. 5d–f; this peak is assigned to Al–O bonding [20].

As-prepared mullite is concluded to have higher Al_2O_3 content than stoichiometric mullite, because the 1120 cm^{-1} absorption peak appeared in the i.r. spectrum, Fig. 5a [4, 21]. Low and McPherson [14] thought that such non-stoichiometric mullite corresponds to the pseudo-tetragonal phase, with composition close to $2Al_2O_3 \cdot SiO_2$. The exothermic effect at 920–950 °C in the DTA curve is attributed to the formation of non-stoichiometric mullite from the Al–Si spinel, and/or to the formation of Al–Si spinel from the amorphous material [7, 8]. Non-stoichiometric mullite reacts with amorphous SiO_2 at ~ 1200 °C to change into stoichiometric mullite (orthorhombic system). A typical reaction process is expressed as follows

$$3(2Al_2O_3 \cdot SiO_2) + SiO_2(\text{amorphous}) \rightarrow 2(3Al_2O_3 \cdot 2SiO_2) \quad (1)$$

This phenomenon is confirmed by the fact that the absorption peak started to shift from 1120 to 1170 cm^{-1} at ~ 1200 °C; splitting of the (1 2 0) and (2 1 0) reflections at and above 1300 °C corresponds to the formation of stoichiometric mullite [14, 22].

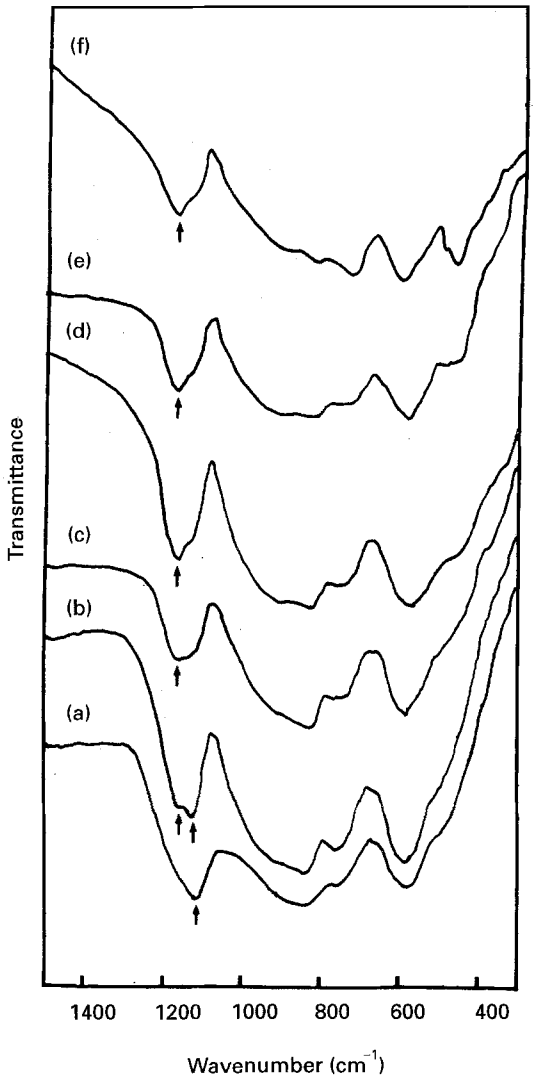

Figure 5 I.r. spectra of the powders calcined at various temperatures: (a) as-prepared powder, (b) 1200 °C for 1 h, (c) 1300 °C for 1 h, (d) 1400 °C for 1 h, (e) 1500 °C for 1 h, and (f) 1700 °C for 1 h at a heating rate of 10 °C min^{-1}. Arrows indicate the absorption peak at 1120 and 1170 cm^{-1}.

Moreover, the change in composition from $2Al_2O_3 \cdot SiO_2$ to $3Al_2O_3 \cdot 2SiO_2$ may also be confirmed by contraction of the cell dimension of the *a*-axis, e.g. 0.7572 nm at 1200 °C and 0.7535 nm at 1400 °C [14, 23]. Non-stoichiometric mullite itself may also decompose to form stoichiometric mullite and α-Al_2O_3 at 1400 °C [14]. The decomposition process is expressed as follows

$$2(2Al_2O_3 \cdot SiO_2) \rightarrow (3Al_2O_3 \cdot 2SiO_2) + \alpha\text{-}Al_2O_3 \quad (2)$$

The residual Al–Si spinel, which has been delayed in ordering and redistribution of Al and Si atoms, also transforms to stoichiometric mullite at ~ 1300 °C [14]. Amorphous SiO_2 must be present up to 1700 °C to retain the mullite composition, because α-Al_2O_3 was detected even at this temperature.

3.2.2. Changes in the powder's properties during calcination

Fig. 6 shows the changes in specific surface area and true density with calcination temperature. The surface area decreased from 40 to < 1 m^2 g^{-1} with increasing

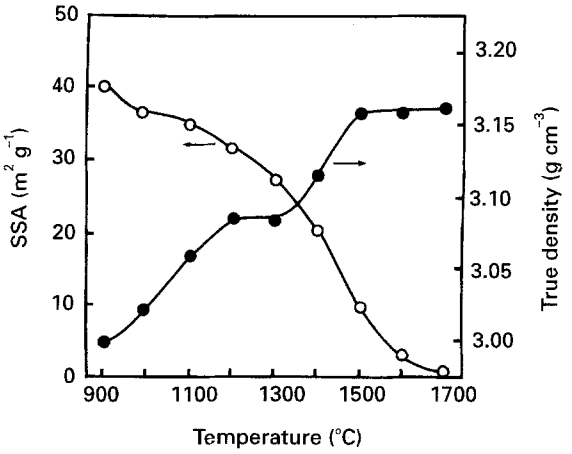

Figure 6 Changes in (○) specific surface area (SSA) and (●) true density of the powder with calcination temperature: calcination time 1 h; heating rate 10 °C min^{-1}.

temperature from 900 to 1700 °C. On the other hand, the true density rose from 3.00 to 3.07 g cm^{-3}, from 900 to 1200 °C, and became almost constant at 1300 °C. Although the true density rose again from 3.07 up to 3.16 g cm^{-3} from 1200 to 1500 °C, it stayed constant on further heating.

Such increases of the true density are divided into two stages: (i) 900–1300 °C, and (ii) 1400–1700 °C; these can be correlated with the reaction products present in the calcined powders. In region (i), 900–1300 °C, the true density may be enhanced, because the crystallinity of non-stoichiometric mullite (density, 3.28 g cm^{-3} [24]) increases; the disappearance of non-stoichiometric mullite and γ-Al_2O_3 (Al–Si spinel, ~ 3.67 g cm^{-3} [12]) at ~ 1300 °C retards the enhancement of the true density. In region (ii), 1300–1700 °C, the true density is enhanced because the amount of stoichiometric mullite (3.16 g cm^{-3}) increases; moreover, the small amount of α-Al_2O_3 (3.99 g cm^{-3}) contributes to enhancing the true density. The true density becomes almost constant at 1500 °C, because it approaches the theoretical density of stoichiometric mullite.

Fig. 7 shows the changes in crystallite size, primary particle size and secondary particle size with calcination temperature. The overall trends reveal that the crystallite, primary particle and secondary particle growths were promoted above 1400 °C. Although the crystallite size was 0.05 μm at 900 °C, it increased with increasing temperature and surpassed 0.1 μm at 1700 °C. The primary particle sizes were larger than the crystallite sizes; they increased from 0.05 to 2 μm with increasing temperature from 900 to 1700 °C. The secondary particle sizes increased from 15 to 90 μm as the temperature increased from 900 to 1700 °C.

On the basis of the above results, the degree of the agglomeration of crystallites per primary particle [DA–CP, $(G_{BET}:G_{XRD})^3$] and of primary particles per secondary particle [DA–PS, $(G_{LSA}:G_{BET})^3$] have been calculated. DA–CP is indicative of whether each primary particle is composed of a single crystal or of several crystallites; whereas DA–PS is indicative of the degree of the bonding strength among primary particles [25]. Fig. 8 shows the changes in DA–CP and

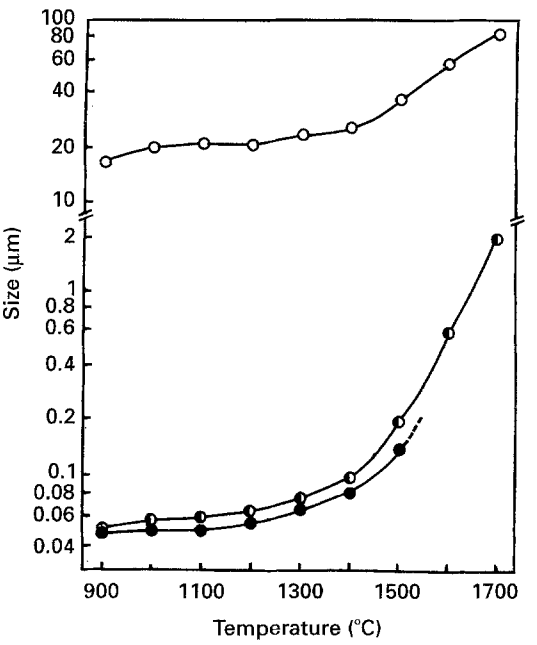

Figure 7 Changes in crystallite size (●), primary particle size (◐) and secondary particle size (○) of the powder with increasing calcination temperature: calcination time, 1 h; heating rate, 10 °C min^{-1}.

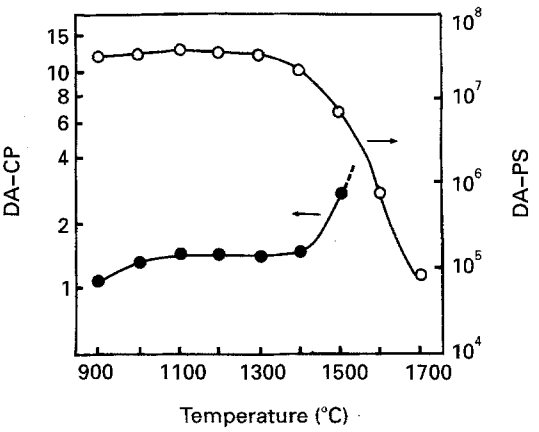

Figure 8 Changes in the degree of agglomeration of (●) crystallite size per primary particle size (DA–CP) and (○) primary particle size per secondary particle size (DA–PS) with increasing calcination temperature: calcination time, 1 h; heating rate, 10 °C min^{-1}.

DA–PS with calcination temperature. Although little change in the DA–CP values was observed in the range 900–1400 °C, the value was enhanced on further heating. The DA–PS values remained unchanged from 900 to 1400 °C; however, they were reduced from 5×10^7 to 10^5 on increasing the temperature from 1400 to 1700 °C.

Some high and low magnification observations by electron microscopy were performed to determine the primary and secondary particle shapes. Fig. 9 shows high magnification TEM and SEM micrographs of the calcined powders. Spherical particles with diameters of ~ 0.1 μm were observed at 900 °C, Fig. 9a; whereas polyhedral particles with sizes of ~ 0.1 μm were present at 1400 °C, Fig. 9b. Polyhedral particles with sizes of ~ 0.2 μm were linked to one another at 1500 °C, Fig 9c. Polyhedral particles with sizes of 0.2

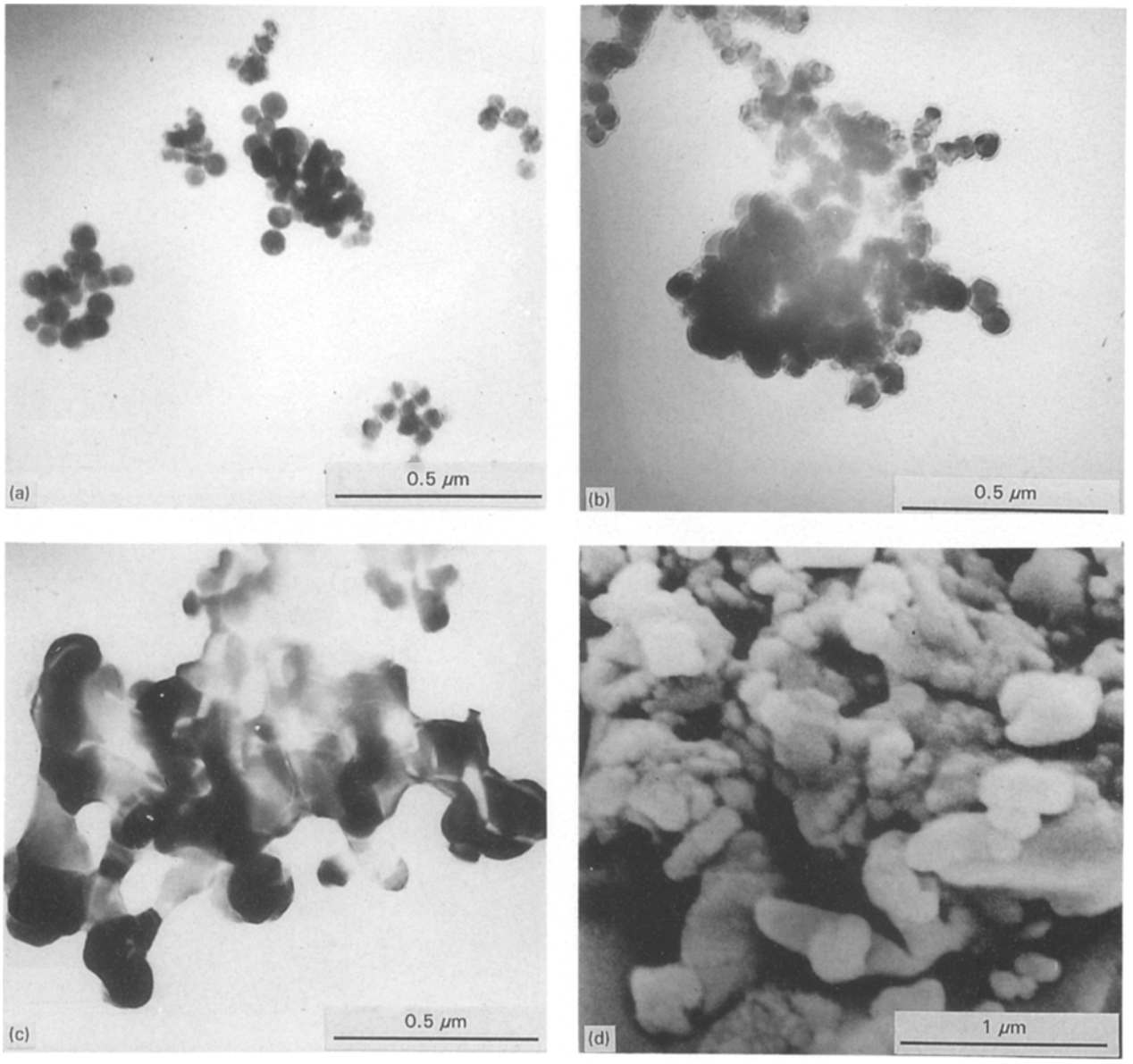

Figure 9 High magnification micrographs of the powders calcined at (a) 900 °C for 1 h, (b) 1400 °C for 1 h, (c) 1500 °C for 1 h, and (d) 1700 °C for 1 h: (a)–(c) are TEM micrographs, (d) is an SEM micrograph.

to 1 μm were linked together to form aggregates at 1700 °C, Fig. 9d.

Fig. 10 shows low magnification SEM micrographs of the calcined powders. Cotton-like agglomerates were observed at 900 °C, Fig 10a. Polyhedral agglomerates with sizes of 10–60 μm were present at 1400 °C, Fig. 10b; the average agglomerate sizes increased from 10–100 to 10–150 μm with increasing temperature from 1500 to 1700 °C, Fig. 10c and d, respectively.

The individual particles observed by high magnification TEM and SEM, Fig 9, correspond to primary particles, because the individual particle sizes agree with the primary particle sizes shown in Fig. 7. A marked change in particle shape at and above 1500 °C may be attributed to sintering of the primary particles; this phenomenon can also be confirmed by the fact that the DA–CP value increased with increasing temperature from 1400 to 1500 °C, Fig. 8.

The agglomerates, with sizes of 10–150 μm, observed by low magnification SEM (Fig. 10) correspond to secondary particles, because they are almost in accord with the secondary particle sizes (Fig. 7). The cotton-like secondary particles at 900 °C appear to be composed of small primary particles; the highest DA–PS value, i.e. 5×10^7, (Fig. 8) suggests that numerous primary particles are present in the secondary particle. Secondary particles with sizes of 10–150 μm at 1700 °C seem to be composed of strongly bonded primary particles; the lowest DA–PS value, i.e. 10^5, at 1700 °C, Fig. 8, indicates that the primary particles coalesced with one another.

As the data on Figs 8–10 indicate, agglomeration of primary particles proceeds at temperatures exceeding 1400 °C. The bonding strength of the primary particles or the agglomerate strength may affect the sinterability of the powder [25]; thus agglomerate strength is evaluated from the data on compressed pressure versus relative density of the compact; the results are shown in Fig. 11. In the case of the powders calcined at (a) 1400 °C, and (b) 1500 °C, the relative density increased exponentially with increasing pressure; however, break points (arrow marks) indicative of the

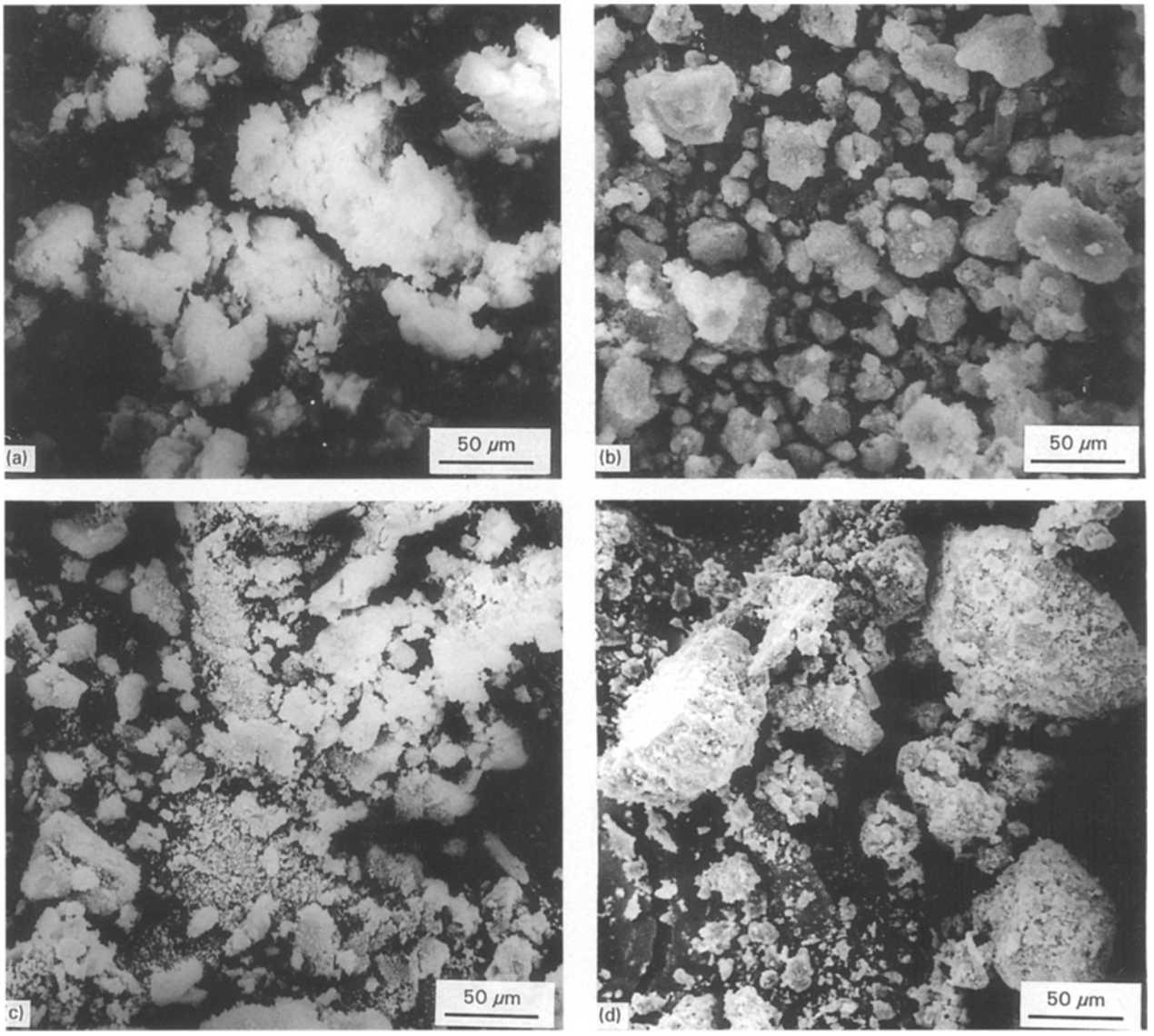

Figure 10 Low magnification SEM micrographs of the powders calcined at (a) 900 °C for 1 h, (b) 1400 °C for 1 h, (c) 1500 °C for 1 h, and (d) 1700 °C for 1 h.

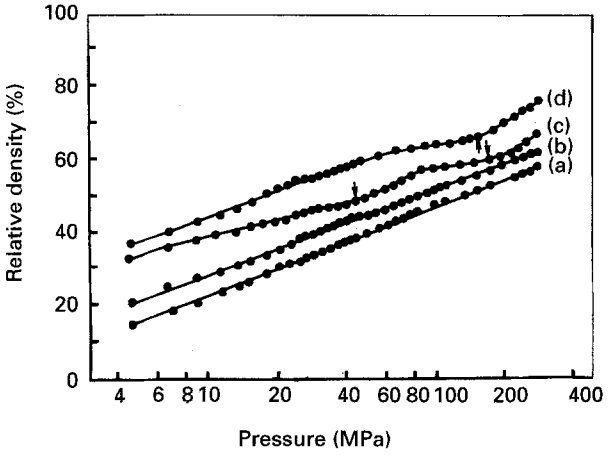

Figure 11 Relationship between relative density (bulk density : true density) and compressed pressure. Calcination conditions: (a) 1400 °C for 1 h, (b) 1500 °C for 1 h, (c) 1600 °C for 1 h, and (d) 1700 °C for 1 h. The arrow marks indicate the break points where the "hard" agglomerates start to fracture.

fracturing of "hard" agglomerates appeared in powders calcined at (c) 1600 °C, and (d) 1700 °C.

Break points which appeared at 1600 and 1700 °C suggest that agglomeration of the primary particles may proceed at and above 1600 °C. Although the primary particles are linked to one another at 1500 °C, Fig. 9c, the bonding strength seems to be weak, because no break point appears in the powder calcined at this temperature. Thus the powders calcined at and below 1500 °C, in which no "hard" agglomerates are included, may have excellent sinterability [26]; details will be described in the next paper.

4. Conclusions

The chemical vapour deposition (CVD) technique, based upon reaction among aluminium chloride ($AlCl_3$) vapour, silicon chloride ($SiCl_4$) vapour and oxygen, was applied to produce a submicrometre-sized mullite ($3Al_2O_3 \cdot 2SiO_2$) powder. The results obtained were as follows.

1. The conditions for preparing crystalline mullite was as follows: (i) reaction temperature, 1200 °C; (ii) carrier gas (Ar) flow rates for $AlCl_3$, 0.3 $dm^3 min^{-1}$, and for $SiCl_4$, 0.3 $dm^3 min^{-1}$; (iii) sublimation temperature of $AlCl_3$, 180 °C, and evaporation temperature of $SiCl_4$, 25 °C; and (iv) flow rate of oxygen, 0.9 $dm^3 min^{-1}$.

2. The as-prepared powder contained mullite, a small amount of γ-Al_2O_3 (Al–Si spinel) and amorphous material, and was composed of spherical primary particles with diameters of ~ 0.05 μm. Although the powder calcined at 1300 °C contained only mullite, the powders calcined at 1400 °C or more contained not only mullite but also α-Al_2O_3. Appreciable increases in crystallite, and in primary and secondary particle sizes were observed at temperatures exceeding 1400 °C.

Acknowledgments

The authors wish to express their thanks to Professor Y. Toda and Dr Ka. Hashimoto for taking the high resolution TEM micrographs.

References

1. A. AKSAY and J. A. PASK, *J. Amer. Ceram. Soc.* **58** (1975) 507.
2. H. SCHNEIDER and E. EBERHARD, *ibid.* **73** (1990) 2073
3. S. KANZAKI, T. KUMAZAWA, J. ASAUMI, O. ABE and H. TABATA, *J. Ceram. Soc. Jpn* **93** (1985) 407.
4. H. SUZUKI, H. SAITO, Y. TOMOKIYO, Y. SUYAMA, in "Ceramic Transactions, Vol. 6 Mullite and Mullite Matrix Composites", edited by S. Somiya, R. F. Davis and J. A. Pask (The American Ceramic Society, Westerville, OH, 1990) p. 263.
5. O. SAKURAI, N. MIZUTANI and M. KATO, *J. Ceram. Soc. Jpn* **96** (1988) 639.
6. K. HAMANO, T. SATO and Z. NAKAGAWA, *J. Ceram. Soc. Jpn* **94** (1986) 818.
7. M. S. J. GANI and R. MCPHERSON, *J. Mater. Sci.* **12** (1977) 999.
8. S. HORI and R. KURITA, in "Ceramic Transactions, Vol. 6, Mullite and Mullite Matrix Composites", edited by S. Somiya, R. F. Davis and J. A. Pask (The American Ceramic Society, Westerville, OH, 1990) p. 311.
9. S-L. CHUNG, Y-C. SHU and M-S. TSAI, in "Ceramic Transactions, Vol. 12, Ceramic Powder Science III", edited by G. L. Messing, S. Hirano and H. Hauser (The American Ceramic Society, Westerville, OH, 1990) p. 275.
10. Powder diffraction file Card No. 8–453 (JCPDS–International Center for Diffraction Data, Swarthmore, PA).
11. Powder diffraction file Card No. 15–776 (JCPDS–International Center for Diffraction Data, Swarthmore, PA).
12. Powder diffraction file Card Nos 10–425 and 29–63 (JCPDS–International Center for Diffraction Data, Swarthmore, PA).
13. I. A. AKSAY, D. M. DABBS and M. SARIKAYA, *J. Amer. Ceram. Soc.* **74** (1991) 2343.
14. I. M. LOW and R. McPHERSON, *J. Mater. Sci.* **24** (1989) 926.
15. K. OKADA and N. OTSUKA, *J. Amer. Ceram. Soc.* **69** (1986) 652.
16. A. K. CHAKRABORTY, *J. Mater. Sci.* **27** (1992) 2075.
17. Y. HIRATA, I. A. AKSAY, R. KURITA, S. HORI and H. KAJI, in "Ceramic Transactions, Vol. 6, Mullite and Mullite Matrix", edited by S. Somiya, R. F. Davis and J. A. Pask (The American Ceramic Society, Westerville, OH, 1990) p. 323.
18. Powder diffraction file Card No. 10–173 (JCPDS–International Center for Diffraction Data, Swarthmore, PA).
19. K. J. D. MACKENZIE, *J. Amer. Ceram. Soc.* **55** (1972) 68.
20. P. COLOMBAN, *J. Mater. Sci.* **24** (1989) 3002.
21. J. S. LEE and S. C. YU, *ibid.* **27** (1992) 5203.
22. H. SCHNEIDER and T. R. LIPINSKI, *J. Amer. Ceram. Soc.* **71** (1988) C-162.
23. W. E. CAMERON, *Amer. Ceram. Soc. Bull.* **56** (1977) 1003.
24. P. D. D. RODRIGO and P. BOCH, *Sci. Ceram.* **13** (1985) C1–405.
25. K. ITATANI, K. KOIZUMI, F. S. HOWELL, A. KISHIOKA and M. KINOSHITA, *J. Mater. Sci.* **24** (1989) 2603.
26. M. D. SACKS and J. A. PASK, *J. Amer. Ceram. Soc.* **65** (1982) 70.

Received 3 February
and accepted 24 June 1994